



Published in final edited form as:

*Sci Transl Med.* 2017 April 12; 9(385): . doi:10.1126/scitranslmed.aak9679.

## Combined antiangiogenic and anti-PD-L1 therapy stimulates tumor immunity through HEV formation

Elizabeth Allen<sup>1,\*</sup>, Arnaud Jabouille<sup>2,\*</sup>, Lee B. Rivera<sup>2</sup>, Inge Lodewijckx<sup>1</sup>, Rindert Missiaen<sup>1</sup>, Veronica Steri<sup>2</sup>, Kevin Feyen<sup>1</sup>, Jaime Tawney<sup>2</sup>, Douglas Hanahan<sup>3</sup>, Iacovos P. Michael<sup>3</sup>, and Gabriele Bergers<sup>1,2,†</sup>

<sup>1</sup>Laboratory of Tumor Microenvironment and Therapeutic Resistance, VIB-Center for Cancer Biology, Department of Oncology, Katholieke Universiteit Leuven, 3000 Leuven, Belgium <sup>2</sup>Brain Tumor Research Center, Department of Neurological Surgery, Helen Diller Family Comprehensive Cancer Center, University of California, San Francisco, San Francisco, CA 94158, USA <sup>3</sup>Swiss Institute for Experimental Cancer Research, School of Life Sciences, Swiss Federal Institute of Technology Lausanne (EPFL), Station 19, 1015 Lausanne, Switzerland

### Abstract

Inhibitors of VEGF (vascular endothelial growth factor)/VEGFR2 (vascular endothelial growth factor receptor 2) are commonly used in the clinic, but their beneficial effects are only observed in a subset of patients and limited by induction of diverse relapse mechanisms. We describe the up-regulation of an adaptive immunosuppressive pathway during antiangiogenic therapy, by which PD-L1 (programmed cell death ligand 1), the ligand of the negative immune checkpoint regulator PD-1 (programmed cell death protein 1), is enhanced by interferon- $\gamma$ -expressing T cells in distinct intratumoral cell types in refractory pancreatic, breast, and brain tumor mouse models. Successful treatment with a combination of anti-VEGFR2 and anti-PD-L1 antibodies induced high endothelial venules (HEVs) in PyMT (polyoma middle T oncoprotein) breast cancer and RT2-PNET (Rip1-Tag2 pancreatic neuroendocrine tumors), but not in glioblastoma (GBM). These HEVs promoted lymphocyte infiltration and activity through activation of lymphotoxin  $\beta$  receptor (LT $\beta$ R) signaling. Further activation of LT $\beta$ R signaling in tumor vessels using an agonistic antibody enhanced HEV formation, immunity, and subsequent apoptosis and necrosis in pancreatic and mammary tumors. Finally, LT $\beta$ R agonists induced HEVs in recalcitrant GBM, enhanced cytotoxic T cell (CTL) activity, and thereby sensitized tumors to antiangiogenic/anti-PD-L1 therapy. Together, our preclinical studies provide evidence that anti-PD-L1 therapy can

<sup>†</sup>Corresponding author: gabriele.bergers@kuleuven.vib.be.

\*These authors contributed equally to this work.

#### SUPPLEMENTARY MATERIALS

[www.sciencetranslationalmedicine.org/cgi/content/full/9/385/eaak9679/DC1](http://www.sciencetranslationalmedicine.org/cgi/content/full/9/385/eaak9679/DC1)

Materials and Methods

**Author contributions:** E.A., A.J., L.B.R., and G.B. designed the experiments. E.A., A.J., L.B.R., I.L., and R.M. performed the experiments, collected and analyzed the data, and interpreted the results. V.S. helped with flow cytometry experiments and performed some immunostainings. K.F. helped with quantitations and performed TC assays. J.T. assisted with immunohistochemical studies. D.H. and I.P.M. generated the B20S antibody and helped with a preclinical RT2-PNET trial. G.B. supervised the research, interpreted the results, and wrote the manuscript with E.A. and with input from other authors.

**Competing interests:** The authors declare that they have no competing interests.

sensitize tumors to antiangiogenic therapy and prolong its efficacy, and conversely, antiangiogenic therapy can improve anti-PD-L1 treatment specifically when it generates intratumoral HEVs that facilitate enhanced CTL infiltration, activity, and tumor cell destruction.

## INTRODUCTION

Sustained angiogenesis and immunosuppression are hallmarks of cancer (1). There is accumulating evidence that these two phenotypes are interconnected and facilitated by shared regulators not only during normal physiological processes, but also in cancer (2). Direct stimulation of the immune system with inhibitors of immune checkpoint regulators, such as antibodies against programmed cell death protein 1 (PD-1) and its ligand, programmed cell death ligand 1 (PD-L1), or cytotoxic T lymphocyte-associated antigen-4 (CTLA-4), has been reported in multiple cancers, resulting in a plethora of ongoing clinical immunotherapeutic trials (3–5). This is based on the observation that cell constituents of tumors can express various surface molecules (such as PD-L1) that engage receptors (such as PD-1) on the surfaces of activated T cells, causing T cell anergy or exhaustion (6, 7). Despite these exciting benefits, only a few patients have responded to these immunotherapies, emphasizing the need to identify strategies that will increase response rates. A prerequisite for successful reversal of tumor-induced immunosuppression is to enable activation and infiltration of tumor antigen-specific T cells into malignant tissues to successfully eradicate tumor and metastatic cells.

Notably, the vasculature is an important regulator of immunity because it controls lymphocyte trafficking. Tumor angiogenic vasculature thwarts the extravasation of tumor-reactive T cells and fosters an immunosuppressive microenvironment that allows tumors to evade host immunosurveillance (8). This is in part achieved by the increased amounts of vascular endothelial growth factor (VEGF) in most cancers, which promotes angiogenesis and impairs leukocyte-endothelial interactions by reducing ICAM-1 (intercellular adhesion molecule-1) and VCAM-1 (vascular cell adhesion molecule-1) adhesion molecules in angiogenic vessels to hinder immune T effector cell infiltration into the tumor (8, 9). VEGF also directly inhibits dendritic cell (DC) maturation and activates antigen-specific regulatory T cells in a neuropilin-1-dependent manner (10, 11). Thus, tumors modify the homeostatic tissue repair program to their advantage by converting immune cells (ICs) from an immune-stimulating to an immunosuppressive and angiogenic phenotype and keeping blood vessels immunosuppressive (2).

The functional importance of VEGF in tumor angiogenesis and in immunosuppression has provided a convincing rationale for the development of inhibitors targeting the VEGF signaling pathway (12–14). Notwithstanding the favorable effects of these inhibitors in some patients, they improve progression-free survival and quality of life, but are unfortunately short-lived and modestly influence overall survival in most patients (12, 15, 16). Several escape mechanisms have been identified that help tumors adapt to the pressures of vascular growth restriction by either reinstating growth by neovascularization or by altering their growth behavior without revascularization (17–24). Studies in numerous preclinical models demonstrate that these adaptations can also be regulated by ICs, which provide an additional

source of chemokines and cytokines to promote angiogenesis, immunosuppression, and other tumor hallmarks (17, 25–28). In this context, we had found that the efficacy of VEGF/VEGF receptor (VEGFR) inhibitors hinged on their ability to induce an immunostimulatory milieu in tumors by repolarizing innate ICs to a T helper 1 (T<sub>H</sub>1) cell phenotype, which was inhibited when phosphatidylinositol 3-kinase (PI3K) was activated in myeloid cells, rendering tumors resistant to antiangiogenic therapy (17). Thus, it is conceivable that additional mechanisms exist to maintain or reinstate a tumor microenvironment that escapes immunosurveillance during treatment.

## RESULTS

### PD-L1 is up-regulated in tumors relapsing from antiangiogenic therapy

To identify immune-related underpinnings of resistance to antiangiogenic therapy, we used three syngeneic tumor models with differing responses to VEGF/VEGFR inhibitors. Antiangiogenic treatment (sorafenib or the anti-VEGFR2 antibody DC101) of 13-week-old mice with a Rip1-Tag2 model of pancreatic neuroendocrine tumors (RT2-PNET), which bear a substantial tumor burden, can transiently reduce vessel density and block tumor growth for about 2 to 3 weeks (response at 15 weeks) followed by reinstatement of neovascularization and robust tumor growth at about 4 weeks of treatment (relapse at 17 weeks). Thus, we can evaluate true response and relapse phases in a single model (17, 19, 26). In the polyoma middle T oncoprotein (PyMT) mammary carcinoma model (MMTV-PyMT, also known as PyMT-BC), angiogenic blockade with DC101 alone slows down tumor growth with some reduction in vessel density (17), whereas NFpp10-glioblastoma (GBM) tumors (deficient in NF1, PTEN, and p53) are resistant to antiangiogenics, which do not elicit significant survival benefits (fig. S1).

Histochemical and fluorescence-activated cell sorting (FACS) analysis of immune checkpoint regulators in the three tumor models revealed a substantial increase of PD-L1<sup>+</sup> cells in refractory PNET and breast cancer (BC), but not in GBM (Fig. 1 and fig. S2). Whereas naïve PNET were devoid of PD-L1<sup>+</sup> cells, with only a subtle increase in tumors undergoing DC101 treatment for 2 weeks, tumors relapsing after 4 weeks of antiangiogenic therapy contained about 11% PD-L1<sup>+</sup> cells (Fig. 1A). Naïve PyMT-BC had about 8% PD-L1<sup>+</sup> cells that doubled after 2 weeks of DC101 therapy (Fig. 1A). Tumor cells (TCs) were the predominant source of PD-L1<sup>+</sup> cells in both tumor types, although endothelial cells (ECs) also expressed PD-L1, which increased during treatment in RT2-PNET and MMTV-PyMT tumors (Fig. 1A and fig. S2). In addition, a small population of CD45<sup>+</sup>PD-L1<sup>+</sup> ICs increased considerably in refractory RT2-PNET and MMTV-PyMT tumors (Fig. 1A and fig. S2). In contrast, CD45<sup>+</sup> ICs were the prevalent PD-L1 population in NFpp10-GBM without substantial difference in the number and composition of PD-L1<sup>+</sup> cells upon VEGF inhibition (B20S) (Fig. 1). These results show that PD-L1 is induced and up-regulated by VEGF/VEGFR inhibitors in different cell constituents in a tumor type-specific manner.

### Interferon- $\gamma$ increases PD-L1 during antiangiogenic therapy

Next, we sought to determine how angiogenic inhibitors increase PD-L1 in tumors. PD-L1 expression can be induced by hypoxia via hypoxia-inducible factor 1 and by interferon- $\gamma$

(IFN $\gamma$ ) (29, 30). Given that antiangiogenic therapy reduces vessel density resulting in enlarged areas of low oxygen tension, we evaluated the percentage of hypoxic cells that displayed PD-L1 expression by staining tumor tissue sections for PD-L1 and the hypoxia-regulated gene carboxic anhydrase IX (CA9) (Fig. 2A) (31). Although tumor hypoxia increased after VEGF blockade in all three model systems, only 2 to 6% of all CA9<sup>+</sup> cells were PD-L1<sup>+</sup>, indicating that hypoxia is not a major cause of PD-L1 up-regulation during antiangiogenic therapy (Fig. 2A). Congruently, hypoxic TCs and ECs from the three different models did not induce PD-L1 in vitro, and bone marrow-derived cells increased PD-L1 after only several hours (fig. S3). In contrast, administration of IFN $\gamma$  strongly up-regulated PD-L1 in all cell types (fig. S3). Because IFN $\gamma$  is predominantly expressed by activated infiltrating T lymphocytes, we isolated CD3<sup>+</sup>CD4<sup>+</sup> and CD3<sup>+</sup>CD8<sup>+</sup> cells from RT2-PNET, PyMT-BC, and NFpp10-GBM tumors in untreated mice and those treated with DC101 or B20S for 2 weeks and determined the percentage of IFN $\gamma$ <sup>+</sup> cells in these populations. IFN $\gamma$ <sup>+</sup>CD8<sup>+</sup> and IFN $\gamma$ <sup>+</sup>CD4<sup>+</sup> cells increased by about twofold upon treatment in RT2-PNET and PyMT-BC, but only IFN $\gamma$ <sup>+</sup>CD8<sup>+</sup> modestly increased by about 50% in GBM (Fig. 2B). Concomitant with IFN $\gamma$  up-regulation, we observed a two- to threefold increase of granzyme B<sup>+</sup> (GzB<sup>+</sup>) CD8<sup>+</sup> cells in RT2-PNET and PyMT-BC upon treatment, indicative of enhanced CD8 activity, whereas NFpp10-GBM tumors contained a low percentage of GzB<sup>+</sup>CD8<sup>+</sup> cells, which only moderately increased after B20S treatment (Fig. 2C). To test whether increased IFN $\gamma$  was responsible for the increase in PD-L1 during antiangiogenic therapy, we isolated PD-L1<sup>+</sup> cells from untreated and anti-VEGF/VEGFR-treated tumors of all three tumor models and sorted them into TCs, ECs, and CD45<sup>+</sup> ICs. We then investigated the expression profile of three well-known IFN $\gamma$ -inducible genes: the chemokine *Cxcl10*, *Mx1* (interferon-induced guanosine 5'-triphosphate-binding protein MX1), and *Ifit3* (interferon-induced protein with tetratricopeptide repeats) (32). Not only was the expression of all three genes higher in PD-L1<sup>+</sup> TCs, ECs, and ICs of RT2-PNET and PyMT-BC compared to their PD-L1<sup>-</sup> counterparts, but VEGF/VEGFR inhibition also substantially increased their expression in PD-L1<sup>+</sup> cells, despite having little overall impact on their expression in PD-L1<sup>-</sup> cell constituents (Fig. 2D). Congruent with the modest cytotoxic T lymphocyte (CTL) activity in NFpp10-GBM, the IFN $\gamma$  response in these tumors was more heterogeneous and subtle. Although PD-L1<sup>+</sup> TCs exhibited increased expression of *Cxcl10*, *Mx1*, and *Ifit3* upon B20S treatment, they comprised only about 2% of all PD-L1<sup>+</sup> cells in GBM (Figs. 1 and 2D). Overall, GBM PD-L1<sup>+</sup> ECs and ICs did not display a significant increase of IFN $\gamma$ -induced genes upon anti-VEGF therapy, and some of these PD-L1<sup>-</sup> cells already had greater expression compared to PD-L1<sup>-</sup> cells from pancreatic and breast tumors (Fig. 2D). Together, these results suggest that PD-L1 expression is increased by IFN $\gamma$ -producing T lymphocytes during VEGF/VEGFR blockade and that the extent of PD-L1 up-regulation correlated with the degree of enhanced CTL activity in the tumors, which was highest in PyMT-BC and RT2-PNET but rather negligible in GBM.

### Anti-PD-L1 therapy sustains response to VEGF blockade in PNET and BC but not in GBM

Our data suggested that the IFN $\gamma$  response in tumors undergoing antiangiogenic therapy elicits a negative and a positive feedback loop. It enhances the differentiation of activated T<sub>H</sub>1 cells to cause an immunostimulating environment but also induces PD-L1 expression that blunts CD8 activity by binding to its receptor PD-1 on T cells, thereby rendering tumors

more immunosuppressive. Therefore, we speculated that inhibition of PD-L1 may be sufficient to prolong an antitumor response during antiangiogenic therapy. To test this proposition, we treated 13-week-old RT2-PNET mice with DC101 or anti-PD-L1 alone or in combination and analyzed tumors after 2 and 4 weeks. After 2 weeks (at 15 weeks of age) with DC101, tumor burden was reduced compared to that of immunoglobulin G (IgG)-treated control mice and anti-PD-L1-treated mice, which succumbed to disease around 15 to 16 weeks of age. After 4 weeks of DC101 treatment, tumors became refractory, as characterized by increased tumor burden (Fig. 3A). In contrast, combined antiangiogenic/anti-PD-L1 therapy impaired tumor regrowth and resulted in a low tumor burden after 4 weeks, which was comparable to 2 weeks of DC101 monotherapy (Fig. 3A). Congruently, combination therapy substantially prolonged overall survival of RT2-PNET mice, whereas DC101 alone only increased progression-free survival, reminiscent of the effects of angiogenic inhibitors in many patients (Fig. 3A and fig. S4) (18). Congruent with our observation that PD-L1<sup>+</sup> cells were rather low in naïve PNET, anti-PD-L1 monotherapy did little to affect the survival of RT2-PNET mice (Fig. 3A and fig. S4). Next, we tested the different treatment combinations in MMTV-PyMT mice. In contrast to the PNET model, DC101 did not elicit a distinct response and a relapse phase in MMTV-PyMT mice but slowed down tumor growth by about 30% (Fig. 3A). Naïve PyMT-BC contain PD-L1<sup>+</sup> cells, and anti-PD-L1 therapy provoked an intermediate response similar to DC101 (Fig. 3A and fig. S4). Moreover, combinatorial treatment of DC101 and anti-PD-L1 was sufficient to substantially restrict tumor growth (Fig. 3A and fig. S4). Finally, we compared antiangiogenic/anti-PD-L1 therapy to the single-treatment modalities in the orthotopic NFpp10-GBM model. Treatment started 10 days after intracranial tumor inoculation. IgG-treated GBM mice and mice undergoing single or combination treatment with B20S and anti-PD-L1 had a median survival of about 26 to 30 days (Fig. 3A and fig. S4). Therefore, in contrast to the improved efficacy of combined neutralization of VEGF/VEGR2 and PD-L1 in the PNET and BC models, anti-PD-L1 therapy was insufficient to sensitize GBM to anti-VEGF therapy.

### Therapy-induced tumor response depends on forming an immunostimulatory milieu

Congruent with our observation that PI3K activation in tumor-infiltrating CD11b<sup>+</sup> cells elicited an immunosuppressive environment and rendered tumors nonresponsive to antiangiogenic therapy (17), we found a substantial increase of pS6 kinase-positive myeloid cells in DC101 refractory PNET tumors, whereas pS6 kinase-positive myeloid cells in DC101/anti-PD-L1-treated tumors remained low, comparable to responding tumors (Fig. 3B). Similarly, DC101, but not DC101/anti-PD-L1 treatment, increased the number of pS6 kinase-positive myeloid cells in PyMT mice in relapsing tumors (D 17W, Fig. 3B). Combination B20S/anti-PD-L1-treated NFpp10-GBM had a somewhat lower number of pS6 kinase<sup>+</sup>CD11b<sup>+</sup> cells compared to those treated with monotherapies, but this was not sufficient to affect survival (Fig. 3, A and B). In support, the expression of immunostimulatory genes was higher than that of immunosuppressive genes in responding, but not relapsing, tumors in all three models (fig. S5A). To further characterize the extent of altered tumor immunity, we evaluated the number and activity of intratumoral T cells in different treatment settings (Fig. 3C). In response to DC101, the numbers of infiltrating CD8<sup>+</sup> T cells increased in RT2-PNET and then dropped to levels comparable to untreated

tumors during relapse. Concomitantly, CD8<sup>+</sup> T cells isolated from responding, but not from untreated or relapsing, tumors exhibited increased amounts of GzB and IFN $\gamma$  proteins (Fig. 3C and fig. S5B). Numbers and activity of CD8<sup>+</sup> T cells were also increased in PyMT-BC undergoing combination therapy, but not in GBM (Fig. 3C and fig. S5B). Finally, we found that enhanced CD8<sup>+</sup> T cell activity closely correlated with enhanced apoptosis in responding, but not refractory, tumors in all three tumor models (Fig. 3, C and D, and fig. S5C). Together, these results revealed that antiangiogenic therapy could sensitize tumors to anti-PD-L1 therapy only when sufficient activated cytotoxic T cells infiltrated the tumors. Thus, anti-VEGF/VEGFR + anti-PD-L1 therapy improved outcome in RT2-PNET and MMTV-PyMT, but not in GBM. These results confirm a recent observation that the extent of intratumoral T cell infiltration and activation in tumors determines the response to PD-L1 blockade (33). DCs are a major source of antigen-presenting cells that activate CD8<sup>+</sup> T cells, and we identified a substantial increase in DC number and activity (measured by dendritic *Cd40*, *Il10*, and *Il12* expression) in RT2-PNET and PyMT-BC, but not GBM, undergoing antiangiogenic/anti-PD-L1 combination therapy (Fig. 4, A and B) (34, 35). Consequently, enhanced intratumoral CD8<sup>+</sup>T cell activity, measured by perforin and GzB expression, was observed in RT2-PNET and PyMT-BC, but again not in GBM (Figs. 3C and 4C).

### **PD-L1 blockade enhances vessel normalization during anti-VEGF therapy in PNET and BC but not in GBM**

The combination treatment with anti-VEGF/VEGFR2 and anti-PD-L1 antibodies stimulated both innate and adaptive IC activation in RT2-PNET and PyMT mice but not in GBM, likely due to the lack of significant T cell infiltration and activation. We wanted to determine why T cells infiltrate PNET and PyMT-BC, but not GBM. A major obstacle for T cell extravasation is the tumor vasculature that restrains intratumoral lymphocyte infiltration and fosters an immunosuppressive microenvironment, which enables tumors to evade host immunosurveillance (8). We therefore hypothesized that differing alterations of the tumor vasculature may be in part responsible for the distinct outcome of antiangiogenic/anti-PD-L1 therapy in the different tumor models.

Analysis of DC101-treated RT2-PNET during the response phase revealed about 50% reduction in vessel density, whereas tumors relapsing from DC101 displayed a vessel density similar to IgG-treated tumors (Fig. 5A). Addition of anti-PD-L1 maintained the low vessel density, thus sustaining the response to DC101 (Fig. 5A). In PyMT and in GBM-bearing mice, VEGF/VEGFR2 inhibition alone or combined with anti-PD-L1 also reduced vessel density in tumors, although the effects in GBM appeared more moderate (Fig. 5A). Congruently, antiangiogenic/anti-PD-L1 treatment increased angiostatic activity of intratumoral myeloid cells in responding tumors (fig. S6). Given that anti-VEGF/VEGFR2 therapy enhances pericyte coverage and normalizes tumor vessels (36–38), we found that all three tumor types that exhibited reduced vessel density during VEGF/VEGFR2 blockade, alone or combined with anti-PD-L1, also displayed tumor vessels with increased NG2<sup>+</sup> and desmin<sup>+</sup> pericyte coverage (Fig. 5B). However, these normalization effects were much more prominent in RT2-PNET and MMTV-PyMT than in NFpp10-GBM.

## Therapy-induced vessel and IC changes are associated with formation of high endothelial venules

We also observed morphological changes in several areas of the tumor vasculature of MMTV-PyMT and RT2-PNET during antiangiogenic/anti-PD-L1 therapy. The vessels appeared thickened with plump ECs rather than the flat ECs of the tumor microvasculature, displaying typical morphological features of high endothelial venules (HEVs) (Fig. 5, C and D). Immunohistochemical analysis revealed that these blood vessels were recognized by MECA79, a well-established antibody that binds all HEVs through a specific carbohydrate epitope but does not react with postcapillary venules, capillaries, or arteries (Fig. 5, C and D) (39). Notably, MECA79<sup>+</sup> vessels exhibited a range of morphological endothelial transformations, and not all displayed plump endothelial appearance, likely reflecting intratumoral heterogeneity in morphology and potential functionality (Fig. 5, C and D, and movies S1 to S3). MECA79<sup>+</sup> vessels were induced only upon DC101/anti-PD-L1 treatment in RT2-PNET, whereas about 20% of tumor vessels in IgG-treated PyMT tumors already expressed MECA79, and this number nearly tripled after combination therapy. In contrast, none of the treatment modalities were able to significantly induce HEVs in GBM (Fig. 5C).

## HEV formation is associated with increased lymphocyte infiltration and activation

These results support the proposition that the beneficial effects of antiangiogenic/anti-PD-L1 therapy may be dependent on intratumoral HEV formation. HEVs are specialized postcapillary venules with portals through which blood-borne lymphocytes enter into secondary lymphoid organs (39, 40). Thus, we hypothesized that therapy-induced intratumoral HEVs may have functional similarities to normal HEVs in lymph nodes and enhance T cell infiltration in tumors, thus facilitating an improved tumor response to antiangiogenic/anti-PD-L1 therapy. Lymphocyte assessment revealed a rather sparse distribution of B and T lymphocytes around MECA79<sup>-</sup> tumor vessels, whereas we observed a 3- to 10-fold increase in the numbers of T and B lymphocytes in the periphery of MECA79<sup>+</sup> HEVs in both PyMT-BC and RT2-PNET across all cohorts (Fig. 6A).

A recent transcriptional profiling analysis revealed a molecular signature that distinguishes HEVs from capillary endothelium derived from normal lymphoid organs (41). A subset of these genes is transcriptionally induced by the lymphotoxin  $\beta$  receptor (LT $\beta$ R)/noncanonical nuclear factor  $\kappa$ B (NF $\kappa$ B) signaling pathway as depicted in Fig. 6B. Among these are genes that code for chemokines and cytokines implicated in lymphocyte recruitment and migration (Fig. 6C; "EC") of which we found some to be significantly up-regulated in ECs of RT2-PNET and PyMT-BC, but not GBM, during combined VEGF/VEGFR2 and PD-L1 neutralization (Fig. 6C). As shown in the schematic, the expression of these factors is in part induced by LT $\beta$ R, which binds lymphotoxin (LT $\alpha$ 1 $\beta$ 2) or LIGHT (homologous to lymphotoxin, exhibits inducible expression, and competes with herpes simplex virus glycoprotein D for herpes virus entry mediator, a receptor expressed by T lymphocytes). Notably, although LIGHT-expressing DCs are required and sufficient for the induction and maintenance of HEVs in normal lymphoid tissues, LIGHT and LT $\alpha$ / $\beta$  can be induced by a variety of ICs besides DCs, including B and T cells (39, 42–44).

### LT $\beta$ R signaling is implicated in HEV formation during antiangiogenic/anti-PD-L1 therapy

Although it remains to be determined which signaling pathways induce HEVs in cancers, the induction of several LT $\beta$ R-regulated factors, including its ligand LIGHT in HEV<sup>+</sup> tumors upon combinatorial treatment (Fig. 6C), suggested that LT $\beta$ R signaling may also be implicated in the formation and function of intratumoral HEVs. As a proof of principle, we used two commercially available antibodies: an agonistic antibody that activates LT $\beta$ R and an antagonistic antibody to block its activation (Fig. 7A) (45–47). LT $\beta$ R antagonist or agonist treatment had no direct effects on TCs (fig. S7). Addition of the LT $\beta$ R agonist during 2 weeks of antiangiogenic/anti-PD-L1 therapy doubled and quadrupled the HEV formation in PyMT-BC (Fig. 7B) and RT2-PNET (fig. S8A), respectively. HEV numbers in the different treatment arms correlated well with the infiltration and activity of CD8<sup>+</sup> T cells, being highest after combination treatment with LT $\beta$ R agonist and lowest after combination with the LT $\beta$ R antagonist (Fig. 7, C and D, and fig. S8B). Tumor burden in RT2-PNET mice was lower compared to control groups but not significantly different among therapy groups due to the short treatment duration (fig. S8C). In contrast, the LT $\beta$ R antagonist reduced HEV back to baseline in naïve PyMT tumors and completely abrogated HEVs in RT2-PNET (Fig. 7B and fig. S8D). Of note, LT $\beta$ R activation alone gave rise to HEVs, although not as much as in combination with antiangiogenic immunotherapy, whereas the LT $\beta$ R antagonist completely blocked HEV formation in both tumor types (fig. S8, D and E). Notably, addition of the LT $\beta$ R agonist not only further increased HEV numbers, but also increased lymphocyte infiltration per HEV, suggesting that LT $\beta$ R signaling contributes to the maturation and functionality of intratumoral HEV (fig. S8, F and G). As a consequence, there was an increase in apoptosing cells and necrotic areas in the double-treated tumors that were further enhanced by addition of the LT $\beta$ R agonist, whereas addition of antagonist decreased apoptosis and had no effect on necrosis (Fig. 7, E and F). Finally, long-term treatment of PyMT mice with anti-VEGFR2/anti-PD-L1 combination alone or in the presence of LT $\beta$ R agonist resulted in tumor stasis, whereas treatment of PyMT mice with IgG was terminated at 3 weeks because of excessive tumor burden (Fig. 7G). The fact that treated tumors exhibited substantial necrosis that still was not cleared efficiently after 3 weeks may explain why tumor sizes did not differ between both combinatorial treatments (Fig. 7F). Together, these results revealed that LT $\beta$ R signaling contributes to tumor HEV generation and that its activation, as assessed by the HEV signature profile, may be more prominent in PyMT-BC than in RT2-PNET undergoing anti-VEGFR2/anti-PD-L1 therapy.

### Activation of LT $\beta$ R signaling in GBM facilitates a response to combined anti-PD-L1 and anti-VEGF therapy by inducing HEVs

The results of our study imply that antiangiogenic/anti-PD-L1 therapy failed in GBM because HEVs did not form to provide sufficient T cell infiltration and activation. If HEV formation is a key mediator of tumor response, then imposed HEV development in GBM should sensitize the tumors to the therapy. LT $\beta$ R activation during antiangiogenic/anti-PD-L1 therapy altered about 15% of tumor vessels into HEVs (Fig. 7H). This was in concordance with a nearly 10-fold increase of GzB<sup>+</sup>-activated CD8<sup>+</sup> cells in GBM (Fig. 7I). Neither LT $\beta$ R activation alone nor antiangiogenic/anti-PD-L1 treatment affected tumor growth, but the combination of both treatment modalities reduced tumor burden by more than 60% (Fig. 7J). These results revealed that recalcitrant tumors, such as GBM, can be

sensitized to immunomodulating and potentially other therapies when intratumoral HEVs can be therapeutically induced.

## DISCUSSION

Here and in a companion study in this issue by Schmittnaegel *et al.* (48), we describe the up-regulation of PD-L1, the ligand of the negative checkpoint regulator PD-1 found on T cells, as an adaptive immunosuppressive mechanism that limited the efficacy of antiangiogenic agents. Thus, although T cells become activated, expressing IFN $\gamma$  during successful antiangiogenic therapy, a negative feedback loop was created by inducing PD-L1 and by blunting T cell activity. Concurrent blockade of angiogenesis and PD-L1 had improved efficacy and prolonged survival when HEVs were induced in tumors, facilitating enhanced T cell infiltration and activation and producing successful eradication of malignant cells.

Mechanistically, the combination therapy can directly counteract the therapy-induced adaptive immunosuppressive pathway (PD-L1 up-regulation) by CTL-secreted IFN $\gamma$ , but it is also conceivable that it unleashes the generation and expansion of new CTLs generated during antiangiogenic therapy, which are then suppressed by PD-L1/PD-1 checkpoint regulation. The negative feedback loop, entailing the interaction of adaptive ICs with PD-L1<sup>+</sup> tumor and host cells, is in line with our former observation (17) that the efficacy of VEGF/VEGFR inhibitors depended on forming an immunostimulatory environment, in part by converting innate ICs to an angiostatic and immunostimulatory phenotype. Moreover, tumors consistently reinforce mechanisms that reinitiate angiogenesis and escape immunosurveillance, in part by activating PI3K $\gamma$  in intratumoral myeloid cells, resulting in tumor relapse (17). The reinstated immunosuppression mediated by PI3K $\gamma$ <sup>+</sup> myeloid cells was also described as a resistance mechanism to CTLA-4 or PD-1 checkpoint inhibitors (49) and supports our finding that response to antiangiogenic/anti-PD-L1 therapy is associated with a low number of PI3K $\gamma$ -activated tumor-associated innate ICs. Further confirmation stems from a clinical study in which enhanced PD-L1 expression and an immunosuppressive tumor microenvironment correlated with resistance to angiogenic inhibitors in metastatic renal cell carcinomas (50). Together, these results support the notion that antiangiogenic therapy causes both adaptive and innate immune responses in tumors to overcome growth restrictions and escape immunosurveillance. Our results also show that antiangiogenic therapy can sensitize PD-L1<sup>-</sup> tumors to checkpoint blockade by inducing PD-L1 expression in tumors.

Naïve RT2-PNET expressed very low amounts of PD-L1, and therefore, anti-PD-L1 monotherapy had no effect in RT2-PNET mice, whereas combined VEGFR2/PD-L1 inhibition produced sustained response and prolonged survival. In light of these results, it is tempting to speculate that there may be a threshold fraction of PD-L1<sup>+</sup> cells in tumors that is required to produce anti-PD-L1 therapeutic efficacy and that inhibition of PD-L1<sup>+</sup> TCs may convey stronger responses than targeting PD-L1<sup>+</sup> host cells. Retrospective clinical studies have shown correlations between tumor PD-L1 expression and response to PD-1/PD-L1 checkpoint blockade therapy (51, 52). In addition, sufficient T cell infiltration in human tumors appeared to be a rate-limiting step for responses to PD-L1 blockade (33, 53). Concordantly, combined antiangiogenic/anti-PD-L1 therapy improved the antitumor

response and resulted in higher T cell infiltration than the single-treatment arms. Moreover, the lack of T cell infiltration was correlated with an ineffective response to combined antiangiogenic/anti-PD-L1 therapy in GBM. These findings support a recent study indicating that adequate T cell infiltration, rather than PD-L1 expression, determines tumor response to checkpoint inhibitors (33). Thus, we wanted to identify the determining factor for sufficient T cell infiltration into tumors.

The tumor vasculature is a major barrier for lymphocytes because it also up-regulates PD-L1 and down-regulates the lymphocyte adhesion molecules ICAM-1 and VCAM-1 that together hinder T cell activation and infiltration into the tumor (9, 11). Consequently, tumor-infiltrating T cells are generally absent or sparse in tumors; however, their presence is prognostic and predictive of response to standard therapies in many tumor types (54, 55). Because intratumoral CD8<sup>+</sup> T cell infiltration is a rate-limiting step for therapeutic success, the question arises whether modulation of the immunosuppressive vasculature would be a suitable strategy to enhance CTL infiltration and subsequent eradication of TCs. In line with this concept, antiangiogenic therapy normalizes tumor blood vessels, albeit transiently, resulting in better blood and oxygen flow and possibly also more efficient T cell extravasation from the blood into the tumor (56, 57). We found that vessel normalization by VEGF/VEGFR inhibitors alone modestly enhanced T cell infiltration (17), but transformation of tumor blood vessels into HEVs substantially increased lymphocyte infiltration. Recent studies have discovered that various human cancers can spontaneously develop areas of HEVs and that their presence correlates with reduced tumor size and improved patient outcome (58, 59). Collectively, therapeutic induction of HEVs with antiangiogenic/anti-PD-L1 therapy promoted antitumor immunity by recruiting more activated lymphocytes into the tumor, thus allowing the local generation and expansion of tumor-destroying lymphocytes that formed centers around HEVs, being reminiscent of tertiary lymphoid structures (TLS).

With regard to the underlying mechanisms of HEV induction in tumors, what is currently known is that CD11c<sup>+</sup> DCs appear to be essential for the maintenance of HEVs in lymphoid organs (39). DCs and other ICs, including activated T cells, express lymphotoxins (LT $\alpha$ , 1 $\beta$ 2 or LIGHT) that stimulate the LT $\beta$ R in ECs to induce the expression of various chemokines and vascular-associated adhesion molecules, which drive HEV formation and T cell recruitment during development (39, 42–44). Ablation of DCs, pharmacological inhibition, or genetic deletion of LT $\beta$ R in ECs is sufficient to impair formation of HEVs in lymphoid organs (43, 60, 61). Multiple lines of evidence indicate that LT $\beta$ R signaling may also be involved in the regulation of the HEV phenotype and function in tumors undergoing antiangiogenic/anti-PD-L1 therapy. First, several endothelial-derived factors, identified in a HEV signature and induced by LT $\beta$ R, are up-regulated during antiangiogenic/anti-PD-L1 therapy in HEV<sup>+</sup> tumors (41, 62). Second, LIGHT is substantially induced in DCs of HEV<sup>+</sup> tumors undergoing combination therapy, although this does not reflect the absolute levels of all lymphotoxin ligands in the tumor. Third, an LT $\beta$ R agonist could further enhance HEV formation, whereas an LT $\beta$ R antagonist lowered and even blocked HEV formation in breast and pancreatic tumors, respectively, undergoing antiangiogenic/anti-PD-L1 therapy.

Notably, activation of LT $\beta$ R was sufficient to induce HEVs and enhance intratumoral activated T cells in GBM and thereby sensitized tumors to antiangiogenic/anti-PD-L1 therapy. These results are encouraging and supported by recent findings that addition of an engineered LIGHT protein to anti-PD-L1 therapy enhanced T cell infiltration and prevented resistance to PD-L1 blockade (33). Recently, intratumoral delivery of a LIGHT peptide was able to normalize tumor vessels and improve tumor perfusion by reestablishing tight pericyte-vessel alignment (63). These studies support the hypothesis that vascular normalization may be a first step to promote HEV formation. Together, these data suggest that antiangiogenic/anti-PD-L1 therapy generates an immunostimulating environment that induces LT $\beta$ R signaling and, together with vascular normalization, triggers HEV formation. These results also raise more questions specifically with regard to termination of therapy, which we have not addressed. How stable are intratumoral HEVs and will the composition and nature of surrounding lymphocytes forming TLS change? If HEVs are solely gates of lymphocyte entry, would then infiltrating ICs become immunosuppressive again, or is an immunostimulating environment also a key for the formation of HEVs and subsequent TLS? In support of this hypothesis, a different RT2 line derived from an independent transgene insertion (Rip1-Tag5), produces an immune response to T antigen, which is associated with the formation of HEV-like structures in islets and tumors (64).

To date, our preclinical studies provide evidence that anti-PD-1 or anti-PD-L1 therapy can sensitize and prolong efficacy of antiangiogenic therapy, and conversely, antiangiogenic therapy can improve anti-PD-L1 treatment by supporting vascular changes, such as vessel normalization and HEV formation, that facilitate enhanced CTL infiltration, activity, and TC destruction. Thus, combined antiangiogenic and checkpoint inhibitors should generate more durable effects and likely sensitize resistant tumors to antiangiogenic therapy when intratumoral HEVs are formed. Several clinical trials combining angiogenic inhibitors and checkpoint blockers are ongoing, and some have produced encouraging results. For example, a small phase 1 study combining the immune checkpoint antibody ipilimumab with the angiogenesis inhibitor antibody bevacizumab showed promising results in advanced melanoma patients with durable patient responses for more than 6 months (65–67). These favorable outcomes were associated with increased expression of the adhesion molecules ICAM-1 and VCAM-1 in ECs and lymphocyte infiltration (68). Because these results are congruent with our observations, it is intriguing to speculate that the formation of intratumoral HEVs, which abundantly express ICAM-1 and VCAM-1 adhesion molecules, may be responsible for the enhanced lymphocyte infiltration observed in these patients.

## MATERIALS AND METHODS

### Study design

The aim of the study was to assess the impact of the combined antiangiogenic/immunotherapy in solid tumors. Angiogenesis inhibitors are used as standard therapy in many cancers and can act as major immune modulators (2), and we examined how they affect tumor response to immune checkpoint therapy and particularly how the PD-1/PD-L1 axis regulates CTL suppression. The efficacy of antiangiogenic and anti-PD-L1 combination alone or with LT $\beta$ R agonists/antagonists was evaluated in mice bearing pancreatic

neuroendocrine tumors (RT2-PNET), mammary carcinomas (MMTV-PyMT), or glioblastoma (NFpp10-GBM). Whereas RT2-PNET respond well, but transiently, to antiangiogenic therapy, MMTV-PyMT and NFpp10-GBM-bearing mice only modestly responded to angiogenic inhibitors (17). Sample size was determined with the University of California, San Francisco (UCSF) Biostatistics and Computational Biology Core to reach statistical significance for tumor burden and mouse survival, which were the primary outcomes used to assess the efficacy of combination therapy. These data were supported by flow cytometry analysis, immunofluorescence staining, and gene expression analysis of the intratumoral immune compartment (T cells, DCs, and myeloid cells) to examine the global immune signature of the tumor response.

Time points for analyses were preselected based on the expected window of efficacy (after 2 weeks of treatment) for single and combination therapy in all models and based on the expected window of antiangiogenic resistance (after 4 weeks of treatment) in the RT2 model. Data include all outliers. Age-matched mice were randomly assigned to experimental cohorts. Biological replicates for cohorts are indicated by *n* in figure legends. Three independent trials were performed for each tumor model. All animal studies were reviewed and approved by the UCSF Institutional Animal Care and Use Committee.

### Tumor models and preclinical trials

RT2-PNET mice (69) were maintained as heterozygotes in the C57BL/6 background, with sucrose-enriched diet starting at 12 weeks of age. Treatment with control rat IgG2a (40 mg/kg; Bio X cell, #BE0089) or DC101 (anti-VEGFR2, 40 mg/kg; Bio X cell, #BE0060) with or without anti-PD-L1 (10 mg/kg; Bio X cell, #BE0101) was initiated at 13 weeks of age and administered twice a week until the mice reached the age of 15 or 17 weeks. For MMTV-PyMT experiments, 100,000 syngeneic PyMT breast TCs (provided by Z. Werb at UCSF) were implanted into the fourth mammary fat pad of female FVB/n mice at 6 to 8 weeks of age. When tumors reached a volume of 250 mm<sup>3</sup>, PyMT mice were treated twice a week for 2 weeks or longer with rat IgG2a or DC101 alone or in combination with anti-PD-L1, with or without anti-LTβR agonist (2 mg/kg) (Abcam, #ab65089) or antagonist (Tebu-Bio, #14971122). For brain tumor experiments, 200,000 NFpp10-GBM TCs (provided by I. Verma at Salk Institute), generated from embryonic C57B/L6 neural stem cells infected with shP53-shNF1 and shPTEN-containing lentiviral vectors (70), were implanted intracranially into the striatum of 7- to 9- week-old female and male syngeneic C57BL/6 mice. One week after implantation, mouse IgG1 (15 mg/kg; Thermo Fischer Scientific, #SA1-35641) or B20S (15 mg/kg; see the Supplementary Materials) treatments with or without anti-PD-L1 or anti-LTβR agonist (2 mg/kg) were administered twice a week for 2 to 4 weeks. For more experimental details, see the Supplementary Materials.

### Statistical analyses

Statistical analyses were performed under the guidance of the Helen Diller Family Comprehensive Cancer Biostatistics and Computational Biology Core using GraphPad Prism (GraphPad software). For mouse survival studies, *P* values were calculated using the log-rank test. For tumor burden, immunostaining, and multicolor flow cytometry, *P* values were calculated using the nonparametric Mann-Whitney test because sample sizes were

small ( $n < 30$ ). Statistical significance was defined by  $P < 0.05$  (two-tailed). Data are presented as means  $\pm$  SEM.

## Supplementary Material

Refer to Web version on PubMed Central for supplementary material.

## Acknowledgments

We thank I. Verma for the NFpp10-GBM cells, Z. Werb for the MMTV-PyMT cell line, D. McDonald for some RT2-PNET mice, F. Stanchi and S. Vinckier for assistance with the two-photon imaging studies, L. Schoonjans and S. Lamy for technical assistance, and R. Ganss and H. Okada for the helpful discussions.

**Funding:** This work was supported by grants from the NIH (U54CA163155, R01CA188404, and R01CA20153), by a Cancer Center Support Grant Developmental RAP award, and by VIB startup funding to G.B.; additional support came from a Human Frontier Science Program fellowship to I.P.M. and a European Research Council Advanced Grant to D.H.

## REFERENCES AND NOTES

- Hanahan D, Weinberg RA. Hallmarks of cancer: The next generation. *Cell*. 2011; 144:646–674. [PubMed: 21376230]
- Motz GT, Coukos G. The parallel lives of angiogenesis and immunosuppression: Cancer and other tales. *Nat Rev Immunol*. 2011; 11:702–711. [PubMed: 21941296]
- Mahoney KM, Rennert PD, Freeman GJ. Combination cancer immunotherapy and new immunomodulatory targets. *Nat Rev Drug Discov*. 2015; 14:561–584. [PubMed: 26228759]
- Callahan MK, Postow MA, Wolchok JD. Targeting T cell co-receptors for cancer therapy. *Immunity*. 2016; 44:1069–1078. [PubMed: 27192570]
- Sharma P, Allison JP. Immune checkpoint targeting in cancer therapy: Toward combination strategies with curative potential. *Cell*. 2015; 161:205–214. [PubMed: 25860605]
- Mellman I, Coukos G, Dranoff G. Cancer immunotherapy comes of age. *Nature*. 2011; 480:480–489. [PubMed: 22193102]
- Gajewski TF, Schreiber H, Fu YX. Innate and adaptive immune cells in the tumor microenvironment. *Nat Immunol*. 2013; 14:1014–1022. [PubMed: 24048123]
- Motz GT, Coukos G. Deciphering and reversing tumor immune suppression. *Immunity*. 2013; 39:61–73. [PubMed: 23890064]
- Dirkx AEM, oude Egbrink MGA, Kuijpers MJE, van der Niet ST, Heijnen VVT, Boumater Steege JCA, Wagstaff J, Griffioen AW. Tumor angiogenesis modulates leukocyte-vessel wall interactions in vivo by reducing endothelial adhesion molecule expression. *Cancer Res*. 2003; 63:2322–2329. [PubMed: 12727857]
- Gabrilovich D, Ishida T, Oyama T, Ran S, Kravtsov V, Nadaf S, Carbone DP. Vascular endothelial growth factor inhibits the development of dendritic cells and dramatically affects the differentiation of multiple hematopoietic lineages in vivo. *Blood*. 1998; 92:4150–4166. [PubMed: 9834220]
- Kandalaf LE, Motz GT, Busch J, Coukos G. Angiogenesis and the tumor vasculature as antitumor immune modulators: The role of vascular endothelial growth factor and endothelin. *Curr Top Microbiol Immunol*. 2011; 344:129–148. [PubMed: 20680802]
- Ferrara N, Adamis AP. Ten years of antivascular endothelial growth factor therapy. *Nat Rev Drug Discov*. 2016; 15:385–403. [PubMed: 26775688]
- Ellis LM, Hicklin DJ. VEGF-targeted therapy: Mechanisms of antitumor activity. *Nat Rev Cancer*. 2008; 8:579–591. [PubMed: 18596824]
- Jayson GC, Kerbel R, Ellis LM, Harris AL. Antiangiogenic therapy in oncology: Current status and future directions. *Lancet*. 2016; 388:518–529. [PubMed: 26853587]

15. Jain RK. Antiangiogenesis strategies revisited: From starving tumors to alleviating hypoxia. *Cancer Cell*. 2014; 26:605–622. [PubMed: 25517747]
16. Vasudev NS, Reynolds AR. Antiangiogenic therapy for cancer: Current progress, unresolved questions and future directions. *Angiogenesis*. 2014; 17:471–494. [PubMed: 24482243]
17. Rivera LB, Meyronet D, Hervieu V, Frederick MJ, Bergsland E, Bergers G. Intratumoral myeloid cells regulate responsiveness and resistance to antiangiogenic therapy. *Cell Rep*. 2015; 11:577–591. [PubMed: 25892230]
18. Bergers G, Hanahan D. Modes of resistance to antiangiogenic therapy. *Nat Rev Cancer*. 2008; 8:592–603. [PubMed: 18650835]
19. Casanovas O, Hicklin DJ, Bergers G, Hanahan D. Drug resistance by evasion of antiangiogenic targeting of VEGF signaling in late-stage pancreatic islet tumors. *Cancer Cell*. 2005; 8:299–309. [PubMed: 16226705]
20. Jiménez-Valerio G, Martínez-Lozano M, Bassani N, Vidal A, Ochoa-de-Olza M, Suárez C, García-del-Muro X, Carles J, Viñals F, Graupera M, Indraccolo S, Casanovas O. Resistance to antiangiogenic therapies by metabolic symbiosis in renal cell carcinoma PDX models and patients. *Cell Rep*. 2016; 15:1134–1143. [PubMed: 27134180]
21. Pàez-Ribes M, Allen E, Hudock J, Takeda T, Okuyama H, Viñals F, Inoue M, Bergers G, Hanahan D, Casanovas O. Antiangiogenic therapy elicits malignant progression of tumors to increased local invasion and distant metastasis. *Cancer Cell*. 2009; 15:220–231. [PubMed: 19249680]
22. Allen E, Miéville P, Warren CM, Saghafinia S, Li L, Peng MW, Hanahan D. Metabolic symbiosis enables adaptive resistance to antiangiogenic therapy that is dependent on mTOR signaling. *Cell Rep*. 2016; 15:1144–1160. [PubMed: 27134166]
23. Ebos JML, Lee CR, Cruz-Munoz W, Bjarnason GA, Christensen JG, Kerbel RS. Accelerated metastasis after short-term treatment with a potent inhibitor of tumor angiogenesis. *Cancer Cell*. 2009; 15:232–239. [PubMed: 19249681]
24. Lu KV, Chang JP, Parachoniak CA, Pandika MM, Aghi MK, Meyronet D, Isachenko N, Fouse SD, Phillips JJ, Cheresch DA, Park M, Bergers G. VEGF inhibits tumor cell invasion and mesenchymal transition through a MET/VEGFR2 complex. *Cancer Cell*. 2012; 22:21–35. [PubMed: 22789536]
25. De Palma M, Anna Venneri M, Galli R, Sergi L, Politi LS, Sampaolesi M, Naldini L. Tie2 identifies a hematopoietic lineage of proangiogenic monocytes required for tumor vessel formation and a mesenchymal population of pericyte progenitors. *Cancer Cell*. 2005; 8:211–226. [PubMed: 16169466]
26. Rigamonti N, Kadioglu E, Keklikoglou I, Wyser Rmili C, Leow CC, De Palma M. Role of angiopoietin-2 in adaptive tumor resistance to VEGF signaling blockade. *Cell Rep*. 2014; 8:696–706. [PubMed: 25088418]
27. Shojaei F, Wu X, Malik AK, Zhong C, Baldwin ME, Schanz S, Fuh G, Gerber HP, Ferrara N. Tumor refractoriness to anti-VEGF treatment is mediated by CD11b<sup>+</sup>Gr1<sup>+</sup> myeloid cells. *Nat Biotechnol*. 2007; 25:911–920. [PubMed: 17664940]
28. Fischer C, Jonckx B, Mazzone M, Zacchigna S, Loges S, Pattarini L, Chorianopoulos E, Liesenborghs L, Koch M, De Mol M, Autiero M, Wyns S, Plaisance S, Moons L, van Rooijen N, Giacca M, Stassen JM, Dewerchin M, Collen D, Carmeliet P. Anti-PlGF inhibits growth of VEGF(R)-inhibitor-resistant tumors without affecting healthy vessels. *Cell*. 2007; 131:463–475. [PubMed: 17981115]
29. Noman MZ, Desantis G, Janji B, Hasmmim M, Karray S, Dessen P, Bronte V, Chouaib S. PD-L1 is a novel direct target of HIF-1 $\alpha$ , and its blockade under hypoxia enhanced MDSC-mediated T cell activation. *J Exp Med*. 2014; 211:781–790. [PubMed: 24778419]
30. Gowrishankar K, Gunatilake D, Gallagher SJ, Tiffen J, Rizos H, Hersey P. Inducible but not constitutive expression of PD-L1 in human melanoma cells is dependent on activation of NF- $\kappa$ B. *PLOS ONE*. 2015; 10:e0123410. [PubMed: 25844720]
31. Hui EP, Chan ATC, Pezzella F, Turley H, To KF, Poon TCW, Zee B, Mo F, Teo PML, Huang DP, Gatter KC, Johnson PJ, Harris AL. Coexpression of hypoxia-inducible factors 1 $\alpha$  and 2 $\alpha$ , carbonic anhydrase IX, and vascular endothelial growth factor in nasopharyngeal carcinoma and relationship to survival. *Clin Cancer Res*. 2002; 8:2595–2604. [PubMed: 12171890]

32. Samarajiwa SA, Forster S, Auchettl K, Hertzog PJ. INTERFEROME: The database of interferon regulated genes. *Nucleic Acids Res.* 2009; 37:D852–D857. [PubMed: 18996892]
33. Tang H, Wang Y, Chlewicki LK, Zhang Y, Guo J, Liang W, Wang J, Wang X, Fu YX. Facilitating T cell infiltration in tumor microenvironment overcomes resistance to PD-L1 blockade. *Cancer Cell.* 2016; 29:285–296. [PubMed: 26977880]
34. Lutz MB. Induction of CD4(+) regulatory and polarized effector/helper t cells by dendritic cells. *Immune Netw.* 2016; 16:13–25. [PubMed: 26937228]
35. Blanco P, Palucka AK, Pascual V, Banchereau J. Dendritic cells and cytokines in human inflammatory and autoimmune diseases. *Cytokine Growth Factor Rev.* 2008; 19:41–52. [PubMed: 18258476]
36. Bergers G, Song S, Meyer-Morse N, Bergsland E, Hanahan D. Benefits of targeting both pericytes and endothelial cells in the tumor vasculature with kinase inhibitors. *J Clin Invest.* 2003; 111:1287–1295. [PubMed: 12727920]
37. Morikawa S, Baluk P, Kaidoh T, Haskell A, Jain RK, McDonald DM. Abnormalities in pericytes on blood vessels and endothelial sprouts in tumors. *Am J Pathol.* 2002; 160:985–1000. [PubMed: 11891196]
38. Jain RK, Booth MF. What brings pericytes to tumor vessels? *J Clin Invest.* 2003; 112:1134–1136. [PubMed: 14561696]
39. Girard JP, Moussion C, Forster R. HEVs, lymphatics and homeostatic immune cell trafficking in lymph nodes. *Nat Rev Immunol.* 2012; 12:762–773. [PubMed: 23018291]
40. Ager A, May MJ. Understanding high endothelial venules: Lessons for cancer immunology. *Oncoimmunology.* 2015; 4:e1008791. [PubMed: 26155419]
41. Lee M, Kiefel H, LaJevic MD, Macauley MS, Kawashima H, O'Hara E, Pan J, Paulson JC, Butcher EC. Transcriptional programs of lymphoid tissue capillary and high endothelium reveal control mechanisms for lymphocyte homing. *Nat Immunol.* 2014; 15:982–995. [PubMed: 25173345]
42. Martinet L, Girard JP. Regulation of tumor-associated high-endothelial venules by dendritic cells: A new opportunity to promote lymphocyte infiltration into breast cancer? *Oncoimmunology.* 2013; 2:e26470. [PubMed: 24482745]
43. Moussion C, Girard JP. Dendritic cells control lymphocyte entry to lymph nodes through high endothelial venules. *Nature.* 2011; 479:542–546. [PubMed: 22080953]
44. Upadhyay V, Fu YX. Lymphotoxin signalling in immune homeostasis and the control of microorganisms. *Nat Rev Immunol.* 2013; 13:270–279. [PubMed: 23524463]
45. Lukashev M, LePage D, Wilson C, Bailly V, Garber E, Lukashin A, Ngamek A, Zeng W, Allaire N, Perrin S, Xu X, Szeliga K, Wortham K, Kelly R, Bottiglio C, Ding J, Griffith L, Heaney G, Silverio E, Yang W, Jarpe M, Fawell S, Reff M, Carmillo A, Miatkowski K, Amatucci J, Crowell T, Prentice H, Meier W, Violette SM, Mackay F, Yang D, Hoffman R, Browning JL. Targeting the lymphotoxin- $\beta$  receptor with agonist antibodies as a potential cancer therapy. *Cancer Res.* 2006; 66:9617–9624. [PubMed: 17018619]
46. Rennert PD, Browning JL, Mebius R, Mackay F, Hochman PS. Surface lymphotoxin alpha/beta complex is required for the development of peripheral lymphoid organs. *J Exp Med.* 1996; 184:1999–2006. [PubMed: 8920886]
47. Wu MY, Wang PY, Han SH, Hsieh SL. The cytoplasmic domain of the lymphotoxin- $\beta$  receptor mediates cell death in HeLa cells. *J Biol Chem.* 1999; 274:11868–11873. [PubMed: 10207006]
48. Schmittnaegel M, Rigamonti N, Kadioglu E, Cassara A, Wyser Rmili C, Kiialainen A, Kienast Y, Mueller H-J, Ooi C-H, Laoui D, De Palma M. Dual angiopoietin-2 and VEGFA inhibition elicits antitumor immunity that is unleashed by PD-1 checkpoint blockade. *Sci Transl Med.* 2017; 9:eaak9670. [PubMed: 28404865]
49. De Henau O, Rausch M, Winkler D, Campesato LF, Liu C, Cymerman DH, Budhu S, Ghosh A, Pink M, Tchaicha J, Douglas M, Tibbitts T, Sharma S, Proctor J, Kosmider N, White K, Stern H, Soglia J, Adams J, Palombella VJ, McGovern K, Kutok JL, Wolchok JD, Merghoub T. Overcoming resistance to checkpoint blockade therapy by targeting PI3K $\gamma$  in myeloid cells. *Nature.* 2016; 539:443–447. [PubMed: 27828943]

50. Liu XD, Hoang A, Zhou L, Kalra S, Yetil A, Sun M, Ding Z, Zhang X, Bai S, German P, Tamboli P, Rao P, Karam JA, Wood C, Matin S, Zurita A, Bex A, Griffioen AW, Gao J, Sharma P, Tannir N, Sircar K, Jonasch E. Resistance to antiangiogenic therapy is associated with an immunosuppressive tumor microenvironment in metastatic renal cell carcinoma. *Cancer Immunol Res.* 2015; 3:1017–1029. [PubMed: 26014097]
51. Herbst RS, Soria JC, Kowanetz M, Fine GD, Hamid O, Gordon MS, Sosman JA, McDermott DF, Powderly JD, Gettinger SN, Kohrt HEK, Horn L, Lawrence DP, Rost S, Leabman M, Xiao Y, Mokatrín A, Koeppen H, Hegde PS, Mellman I, Chen DS, Hodi FS. Predictive correlates of response to the anti-PD-L1 antibody MPDL3280A in cancer patients. *Nature.* 2014; 515:563–567. [PubMed: 25428504]
52. Topalian SL, Hodi FS, Brahmer JR, Gettinger SN, Smith DC, McDermott DF, Powderly JD, Carvajal RD, Sosman JA, Atkins MB, Leming PD, Spigel DR, Antonia SJ, Horn L, Drake CG, Pardoll DM, Chen L, Sharfman WH, Anders RA, Taube JM, McMiller TL, Xu H, Korman AJ, Jure-Kunkel M, Agrawal S, McDonald D, Kollia GD, Gupta A, Wigginton JM, Sznol M. Safety, activity, and immune correlates of anti-PD-1 antibody in cancer. *N Engl J Med.* 2012; 366:2443–2454. [PubMed: 22658127]
53. TumeH PC, Harview CL, Yearley JH, Peter Shintaku I, Taylor EJM, Robert L, Chmielowski B, Spasic M, Henry G, Ciobanu V, West AN, Carmona M, Kivork C, Seja E, Cherry G, Gutierrez AJ, Grogan TR, Mateus C, Tomasic G, Glaspy JA, Emerson RO, Robins H, Pierce RH, Elashoff DA, Robert C, Ribas A. PD-1 blockade induces responses by inhibiting adaptive immune resistance. *Nature.* 2014; 515:568–571. [PubMed: 25428505]
54. Hwang WT, Adams SF, Tahirovic E, Hagemann IS, Coukos G. Prognostic significance of tumor-infiltrating T cells in ovarian cancer: A meta-analysis. *Gynecol Oncol.* 2012; 124:192–198. [PubMed: 22040834]
55. Mahmoud SMA, Paish EC, Powe DG, Macmillan RD, Grainge MJ, Lee AHS, Ellis IO, Green AR. Tumor-infiltrating CD8<sup>+</sup> lymphocytes predict clinical outcome in breast cancer. *J Clin Oncol.* 2011; 29:1949–1955. [PubMed: 21483002]
56. Jain RK. Normalizing tumor vasculature with antiangiogenic therapy: A new paradigm for combination therapy. *Nat Med.* 2001; 7:987–989. [PubMed: 11533692]
57. Jain RK. Normalization of tumor vasculature: An emerging concept in antiangiogenic therapy. *Science.* 2005; 307:58–62. [PubMed: 15637262]
58. Martinet L, Le Guellec S, Filleron T, Lamant L, Meyer N, Rochaix P, Garrido I, Girard JP. High endothelial venules (HEVs) in human melanoma lesions: Major gateways for tumor-infiltrating lymphocytes. *Oncoimmunology.* 2012; 1:829–839. [PubMed: 23162750]
59. Martinet L, Garrido I, Filleron T, Le Guellec S, Bellard E, Fournie JJ, Rochaix P, Girard JP. Human solid tumors contain high endothelial venules: Association with T- and B-lymphocyte infiltration and favorable prognosis in breast cancer. *Cancer Res.* 2011; 71:5678–5687. [PubMed: 21846823]
60. Firner S, Onder L, Nindl V, Ludewig B. Tight control—decision-making during T cell—vascular endothelial cell interaction. *Front Immunol.* 2012; 3:279. [PubMed: 22969771]
61. Browning JL, Allaire N, Ngamek A, Notidis E, Hunt J, Perrin S, Fava RA. Lymphotoxin- $\beta$  receptor signaling is required for the homeostatic control of HEV differentiation and function. *Immunity.* 2005; 23:539–550. [PubMed: 16286021]
62. Norris PS, Ware CF. The LT $\beta$ R signaling pathway. *Adv Exp Med Biol.* 2007; 597:160–172. [PubMed: 17633025]
63. Johansson-Percival A, Li ZJ, Lakhiani DD, He B, Wang X, Hamzah J, Ganss R. Intratumoral LIGHT restores pericyte contractile properties and vessel integrity. *Cell Rep.* 2015; 13:2687–2698. [PubMed: 26711337]
64. Onrust SV, Hartl PM, Rosen SD, Hanahan D. Modulation of L-selectin ligand expression during an immune response accompanying tumorigenesis in transgenic mice. *J Clin Invest.* 1996; 97:54–64. [PubMed: 8550850]
65. Ott PA, Hodi FS, Buchbinder EI. Inhibition of immune checkpoints and vascular endothelial growth factor as combination therapy for metastatic melanoma: An overview of rationale, preclinical evidence, and initial clinical data. *Front Oncol.* 2015; 5:202. [PubMed: 26442214]

66. Garber K. Promising early results for immunotherapy-antiangiogenesis combination. *J Natl Cancer Inst.* 2014; 106:dju392. [PubMed: 25421345]
67. Schoenfeld JD, Dranoff G. Antiangiogenesis immunotherapy. *Hum Vaccin.* 2011; 7:976–981. [PubMed: 21860259]
68. Wu X, Giobbie-Hurder A, Liao X, Lawrence D, McDermott D, Zhou J, Rodig S, Hodi FS. VEGF neutralization plus CTLA-4 blockade alters soluble and cellular factors associated with enhancing lymphocyte infiltration and humoral recognition in melanoma. *Cancer Immunol Res.* 2016; 4:858–868. [PubMed: 27549123]
69. Hanahan D. Heritable formation of pancreatic beta-cell tumours in transgenic mice expressing recombinant insulin/simian virus 40 oncogenes. *Nature.* 1985; 315:115–122.
70. Friedmann-Morvinski D, Bushong EA, Ke E, Soda Y, Marumoto T, Singer O, Ellisman MH, Verma IM. Dedifferentiation of neurons and astrocytes by oncogenes can induce gliomas in mice. *Science.* 2012; 338:1080–1084. [PubMed: 23087000]

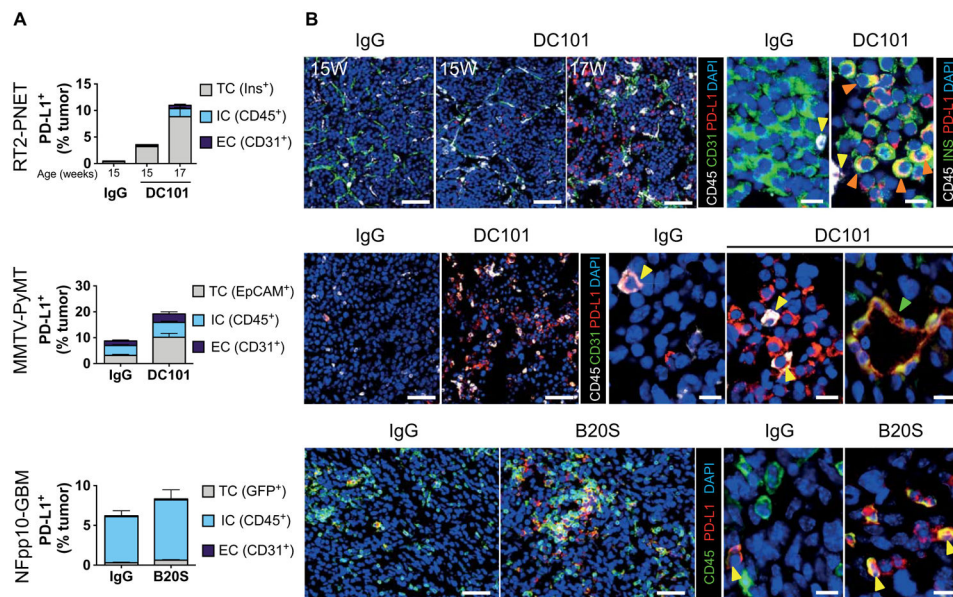


**Fig. 1. Antiangiogenic therapy enhances PD-L1 expression in relapsing tumors**  
**(A)** FACS analysis of PD-L1<sup>+</sup> cell composition of RT2-PNET, MMTV-PyMT, and NFpp10-GBM tumors treated with IgG or angiogenesis inhibitors. RT2-PNET: 15-week-old mice treated with DC101 represent treatment response, and 17-week-old mice represent relapse. Data are presented as means ± SEM. DC101 15W (weeks) versus IgG 15W ( $n = 4$ ),  $P = 0.0286$  for TC,  $P = 0.06571$  for IC, and  $P = 0.0286$  for EC; DC101 17W ( $n = 7$ ) versus IgG 15W ( $n = 4$ ),  $P = 0.0061$  for TC,  $P = 0.0121$  for IC, and  $P = 0.0061$  for EC. MMTV-PyMT: DC101 versus IgG ( $n = 9$ ),  $P < 0.0001$  for TC,  $P = 0.0106$  for IC, and  $P = 0.0423$  for EC. NFpp10-GBM trial: B20S versus IgG ( $n = 7$ ),  $P = 0.0286$  for TC,  $P = 0.0070$  for IC, and  $P = 0.4359$  for EC. Statistical analysis by Mann-Whitney test. **(B)** Immunofluorescence staining of PD-L1<sup>+</sup> cells (red), blood vessels (CD31<sup>+</sup>; green arrows), ICs (CD45<sup>+</sup>; yellow arrows), and RT2-PNET TCs (insulin<sup>+</sup>; orange arrows). Scale bars, 50 μm (left panels); 10 μm (right panels). DAPI, 4', 6-diamidino-2-phenylindole.

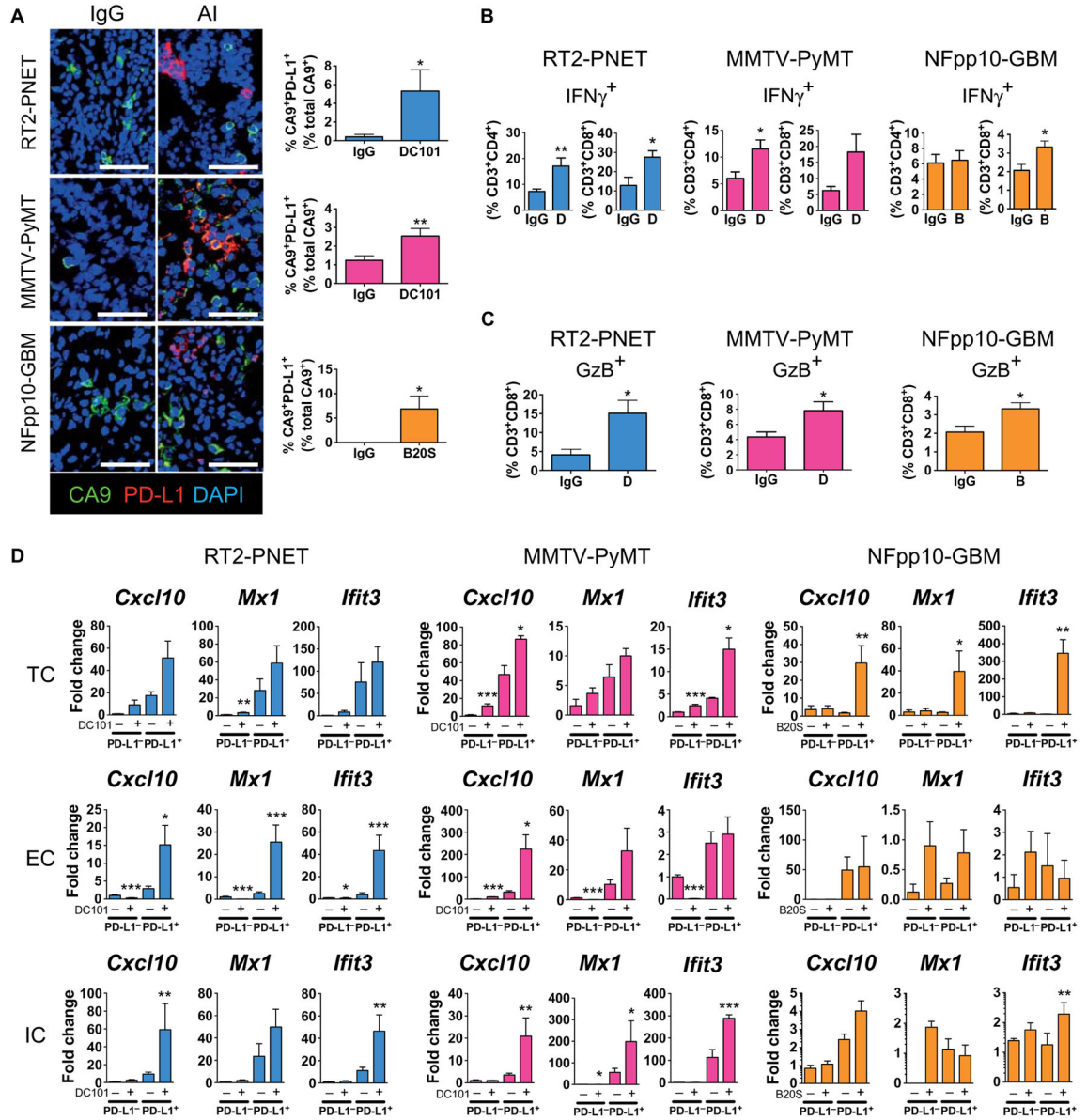


**Fig. 2. IFN $\gamma$ , but not hypoxia, increases PD-L1 expression during antiangiogenic therapy**  
 (A) Immunofluorescence staining and quantitation of the hypoxia marker CA9 and PD-L1 in RT2-PNET (IgG and DC101,  $n = 6$ ), MMTV-PyMT (IgG,  $n = 29$ ; DC101,  $n = 18$ ), and NFpp10-GBM (IgG and B20S,  $n = 5$ ) tumors treated with IgG or angiogenesis inhibitors (AI). Scale bars, 50  $\mu$ m. (B) FACS analysis of IFN $\gamma$ <sup>+</sup>CD3<sup>+</sup>CD4<sup>+</sup> and IFN $\gamma$ <sup>+</sup>CD3<sup>+</sup>CD8<sup>+</sup> T cells in RT2-PNET [IgG and DC101 (D),  $n = 6/6$ ], MMTV-PyMT (IgG,  $n = 6/5$ ; D,  $n = 6/6$ ), and NFpp10-GBM [IgG,  $n = 6/7$ ; B20S (B),  $n = 6/7$ ] tumors. (C) FACS analysis of GzB<sup>+</sup>CD3<sup>+</sup>CD8<sup>+</sup> T cells in RT2-PNET (IgG and D,  $n = 6$ ), MMTV-PyMT (IgG and D,  $n = 9$ ), and NFpp10-GBM (IgG,  $n = 8$ ; B,  $n = 9$ ) tumors. (D) Quantitative polymerase chain reaction (qPCR) analysis of IFN $\gamma$ -mediated genes *Cxcl10*, *Mx1*, and *Ifit3* in FACS-sorted PD-L1<sup>-</sup> or PD-L1<sup>+</sup> TCs, ECs, and ICs from RT2-PNET (TC, EC, and IC,  $n = 8$ ), MMTV-PyMT (TC, EC, and IC,  $n = 8$ ), and NFpp10-GBM (TC, EC, and IC,  $n = 4$ ) tumors. For primers, see

table S1. Data are presented as means  $\pm$  SEM. \* $P < 0.05$ , \*\* $P < 0.01$ , and \*\*\* $P < 0.001$  (for exact  $P$  values, see table S2); Mann-Whitney test. Black asterisks represent  $P$  values for comparisons between IgG and DC101 or B20S.

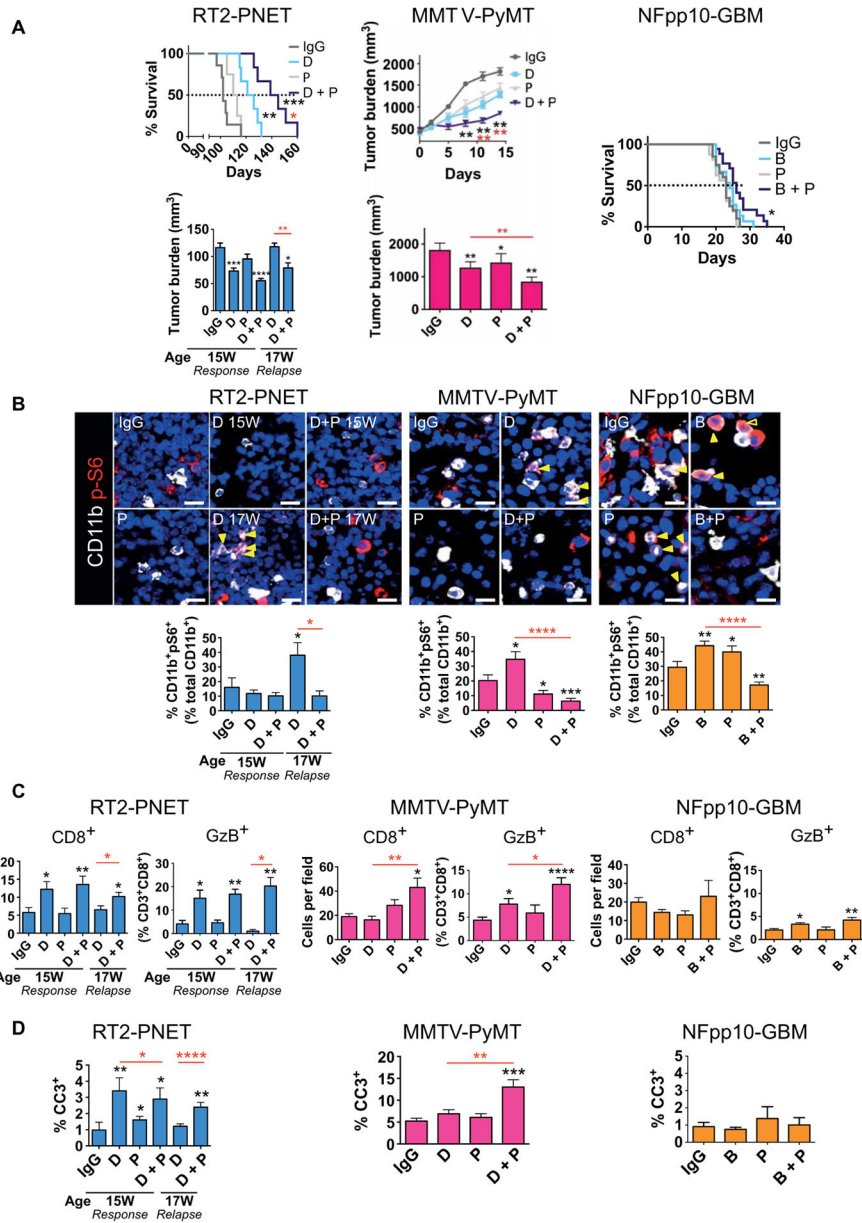


**Fig. 3. Anti-PD-L1 enhances the efficacy of antiangiogenic therapy in RT2-PNET and MMTV-PyMT but not in NFpp10-GBM**

(A) Bottom left: Tumor burden of RT2-PNET, IgG (13 to 15W),  $n = 8$ ; D (13 to 15W),  $n = 8$ ; anti-PD-L1 (P) (13 to 15W),  $n = 8$ ; D + P (13 to 15W),  $n = 11$ ; D (13 to 17W),  $n = 11$ ; D + P (13 to 17W),  $n = 11$ . Top left: Survival of RT2-PNET, IgG,  $n = 10$ ; D,  $n = 10$ ; P,  $n = 10$ ; D + P,  $n = 12$ . Top center: Tumor growth curves. Bottom center: Tumor burden of MMTV-PyMT (2 weeks), IgG,  $n = 6$ ; D,  $n = 6$ ; P,  $n = 6$ ; D + P,  $n = 6$ . Right: Survival of NFpp10-GBM, IgG,  $n = 20$ ; B,  $n = 15$ ; P,  $n = 16$ ; B + P,  $n = 18$ . (B) Immunofluorescence staining (yellow arrows) and quantitation of CD11b<sup>+</sup>pS6<sup>+</sup> cells in RT2-PNET (IgG,  $n = 12$ ; D 15W,  $n = 11$ ; D + P 15W,  $n = 34$ ; D 17W,  $n = 8$ ; D + P 17W,  $n = 15$ ), MMTV-PyMT (IgG,  $n = 20$ ; D,  $n = 24$ ; P,  $n = 20$ ; D + P,  $n = 23$ ), and NFpp10-GBM (IgG,  $n = 15$ ; B,  $n = 20$ ; P,  $n = 20$ ; B

+ P,  $n = 24$ ) tumors. Scale bars, 10  $\mu\text{m}$ . **(C)** Quantitation of CD8<sup>+</sup> and GzB<sup>+</sup> cells in RT2-PNET (IgG,  $n = 9/6$ ; D 15W,  $n = 9/6$ ; P,  $n = 9/6$ ; D + P 15W,  $n = 7/7$ ; D 17W,  $n = 19/4$ ; D + P 17W,  $n = 14/4$ ), MMTV-PyMT (IgG,  $n = 18/9$ ; D,  $n = 20/9$ ; P,  $n = 24/9$ ; D + P,  $n = 18/9$ ), and NFpp10-GBM (IgG,  $n = 15/8$ ; B,  $n = 15/9$ ; P,  $n = 13/7$ ; B + P,  $n = 14/9$ ) tumors. **(D)** Quantitation of apoptotic cleaved caspase 3<sup>+</sup> (CC3<sup>+</sup>) cells in RT2-PNET (IgG,  $n = 8$ ; D 15W,  $n = 15$ ; P,  $n = 20$ ; D + P 15W,  $n = 29$ ; D 17W,  $n = 25$ ; D + P 17W,  $n = 25$ ), MMTV-PyMT (IgG, D, P, and D + P,  $n = 8$ ), and NFpp10-GBM (IgG,  $n = 5$ ; B,  $n = 6$ ; P,  $n = 3$ ; B + P,  $n = 5$ ) tumors. Data are presented as means  $\pm$  SEM. \* $P < 0.05$ , \*\* $P < 0.01$ , \*\*\* $P < 0.001$ , and \*\*\*\* $P < 0.0001$  (for exact  $P$  values, see table S2); Mann-Whitney test or log-rank test for survival. Black asterisks represent  $P$  values for comparisons between IgG and different treatments; red asterisks represent  $P$  values for other comparisons.

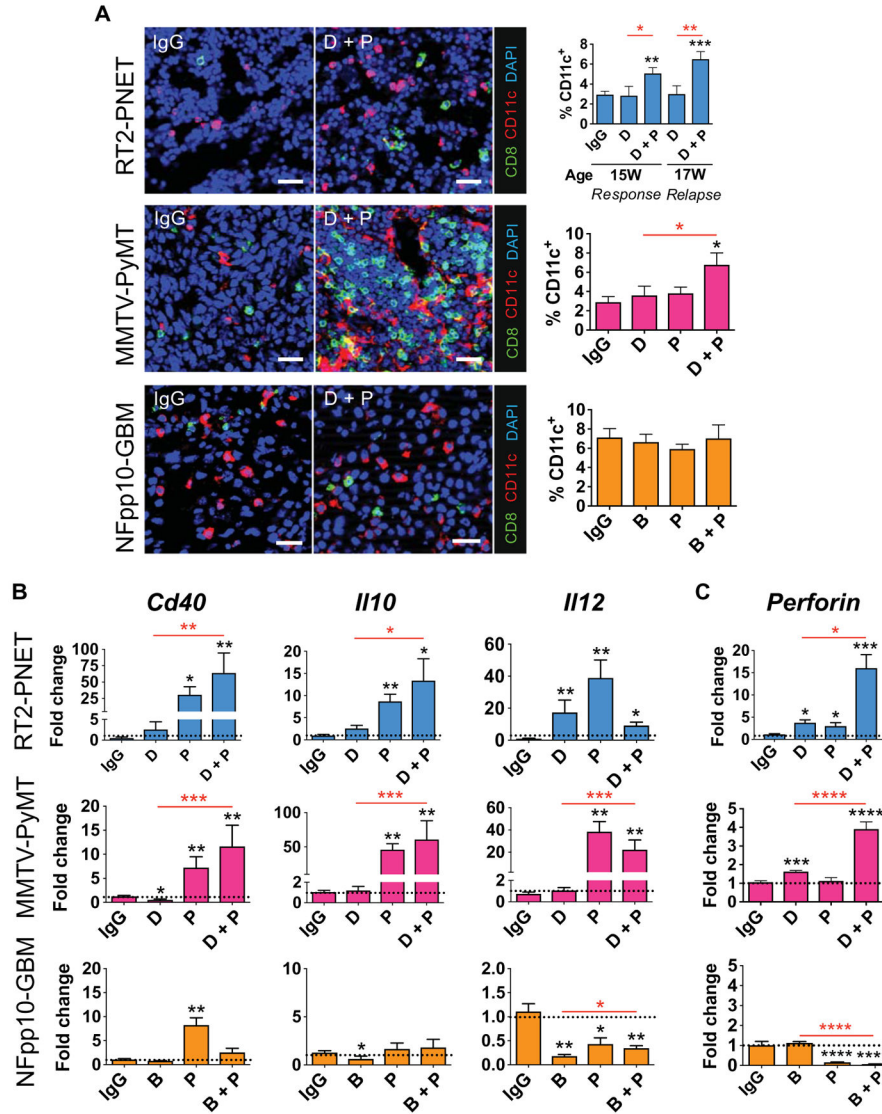


**Fig. 4. Combined anti-PD-L1 and antiangiogenic therapy stimulates infiltration and activation of DCs and CTLs in responding tumors**

(A) Immunofluorescence staining and quantitation of CD8<sup>+</sup> and CD11c<sup>+</sup> cells in RT2-PNET (IgG, *n* = 11; D 15W, *n* = 9; D + P 15W, *n* = 18; D 17W, *n* = 11; D + P, *n* = 13), MMTV-PyMT (IgG, D, P, and D + P, *n* = 20), and NFpp10-GBM (IgG, *n* = 18; B, *n* = 20; P, *n* = 13; B + P, *n* = 14) tumors. Quantitation of CD11c<sup>+</sup> infiltrates is shown on the right. Scale bars, 25 μm. (B) qPCR-based expression analysis of FACS-sorted DCs in RT2-PNET (IgG, *n* = 4; D, *n* = 8; P, *n* = 8; D + P, *n* = 15 to 16), MMTV-PyMT (IgG, *n* = 4; D, *n* = 8; P, *n* = 11; D + P, *n* = 8), and NFpp10-GBM (IgG, *n* = 4; B, *n* = 8; P, *n* = 8; B + P, *n* = 8) tumors. (C) qPCR analysis of perforin in CD3<sup>+</sup>CD8<sup>+</sup> CTLs from RT2-PNET (IgG, *n* = 4; D, *n* = 8; P, *n* = 8; D + P, *n* = 16), MMTV-PyMT (IgG, *n* = 6; D, *n* = 18; P, *n* = 12; D + P, *n* = 16), and NFpp10-GBM (IgG, *n* = 8; B, *n* = 24; P, *n* = 40; B + P, *n* = 32) tumors. Dotted line indicates baseline gene expression in IgG-treated samples. Data are presented as means ± SEM. \**P* < 0.05, \*\**P* < 0.01, \*\*\**P* < 0.001, and \*\*\*\**P* < 0.0001 (for exact *P* values, see table S2); Mann-Whitney

test. Black asterisks represent *P* values for comparisons between IgG and different treatments; red asterisks represent *P* values for other comparisons.

Author Manuscript

Author Manuscript

Author Manuscript

Author Manuscript

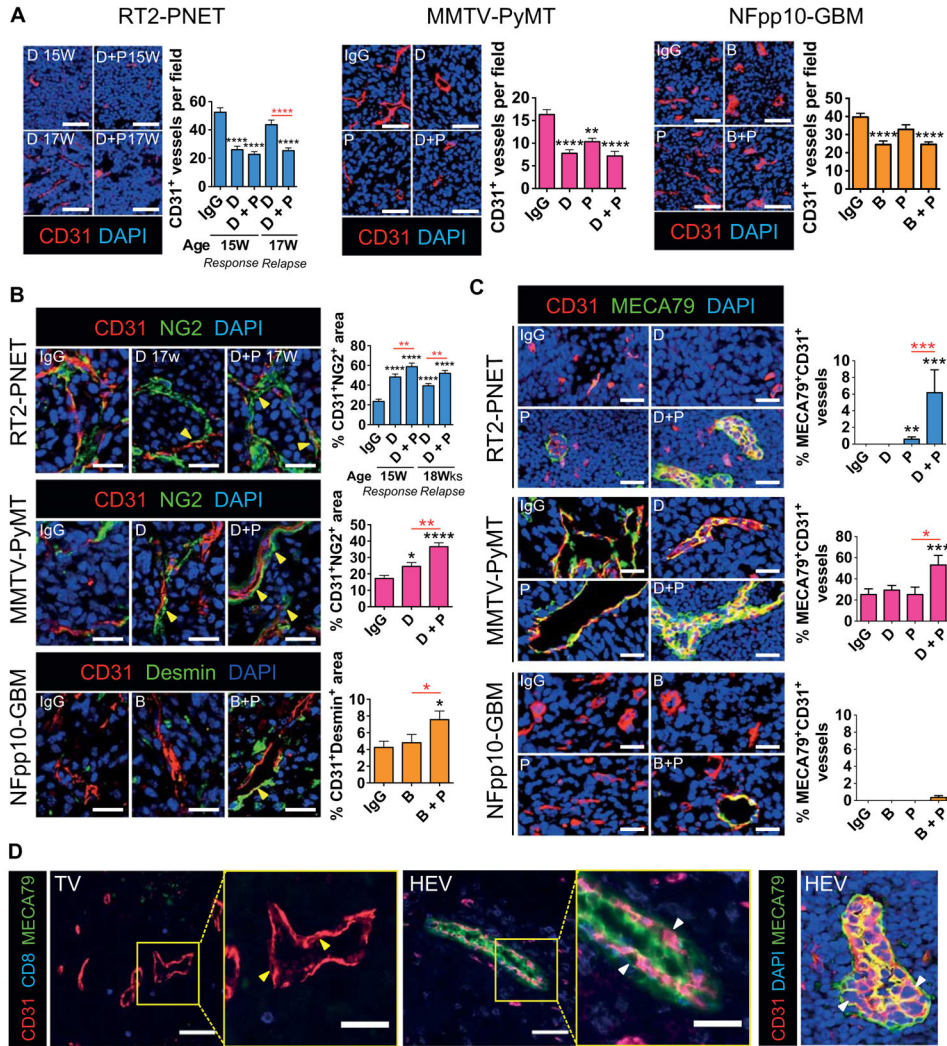


**Fig. 5. Combined antiangiogenic/anti-PD-L1 therapy stimulates vessel normalization and HEV formation in responding tumors**  
**(A)** Visualization and quantification of CD31<sup>+</sup> blood vessels in RT2-PNET (IgG, D, and D + P, *n* = 15), MMTV-PyMT (IgG, *n* = 35; D, *n* = 25; P, *n* = 15; D + P, *n* = 28), and NFpp10-GBM (IgG, *n* = 35; B, *n* = 39; P, *n* = 15; B + P, *n* = 39) tumors. Scale bars, 50  $\mu$ m. **(B)** Immunofluorescence staining of CD31 and NG2 or desmin and quantitation of pericyte-covered blood vessels in RT2-PNET (IgG, D, and D + P, *n* = 15), MMTV-PyMT (IgG, D, and D + P, *n* = 15), and NFpp10-GBM (IgG, B, and B + P, *n* = 15) tumors. Scale bars, 25  $\mu$ m. **(C)** Images and quantitation of CD31<sup>+</sup>MECA79<sup>+</sup> blood vessels in the different tumor types. Scale bars, 25  $\mu$ m. **(D)** Visualization of CD31<sup>+</sup>MECA79<sup>-</sup> [tumor vessels (TV); flat ECs, yellow arrows] and CD31<sup>+</sup>MECA79<sup>+</sup> (HEV; plump ECs, white arrows) tumor vessels. Scale bars, 50  $\mu$ m (low-magnification images); 25  $\mu$ m (high-magnification images). Data are presented as means  $\pm$  SEM. \**P* < 0.05, \*\**P* < 0.01, \*\*\**P* < 0.001, and \*\*\*\**P* < 0.0001 (for exact *P* values, see table S2); Mann-Whitney test. Black asterisks represent *P* values for comparisons between IgG and different treatments; red asterisks represent *P* values for other comparisons.

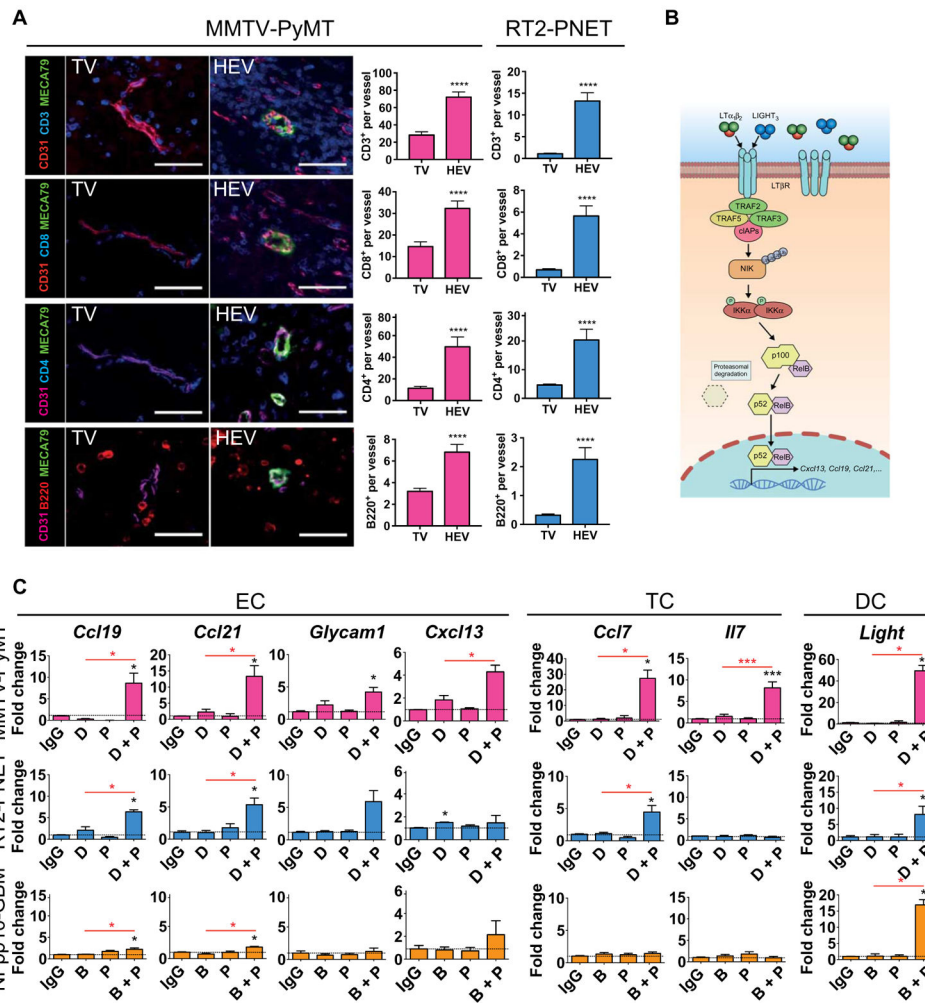


**Fig. 6. Intratumoral HEVs increase lymphocyte infiltration**

(A) Visualization and quantitation of CD3<sup>+</sup>, CD8<sup>+</sup>, and CD4<sup>+</sup> T cells and B220<sup>+</sup> B cells within 50 μm of MECA79<sup>-</sup> tumor vessels (TV) and MECA79<sup>+</sup> tumor vessels (HEV). MMTV-PyMT: TV, *n* = 42; HEV, *n* = 20. RT2-PNET: TV, *n* = 28; HEV, *n* = 12. Scale bars, 50 μm. (B) Schematic of the LTβR/noncanonical NFκB signaling pathway that induces the expression of various HEV signature genes. (C) qPCR-based expression analysis of HEV signature genes in different FACS-sorted cell populations from MMTV-PyMT, RT2-PNET, and NFpp10-GBM. For all genes, *n* = 4 except *Cxcl13* and *Il7*, *n* = 4; *Glycam1*, *n* = 3. Dotted line indicates baseline gene expression in IgG-treated samples. Data are presented as means ± SEM. \**P* < 0.05, \*\**P* < 0.01, \*\*\**P* < 0.001, and \*\*\*\**P* < 0.0001 (for exact *P* values, see table S2); Mann-Whitney test. Black asterisks represent *P* values for comparisons between IgG and different treatments; red asterisks represent *P* values for other comparisons.

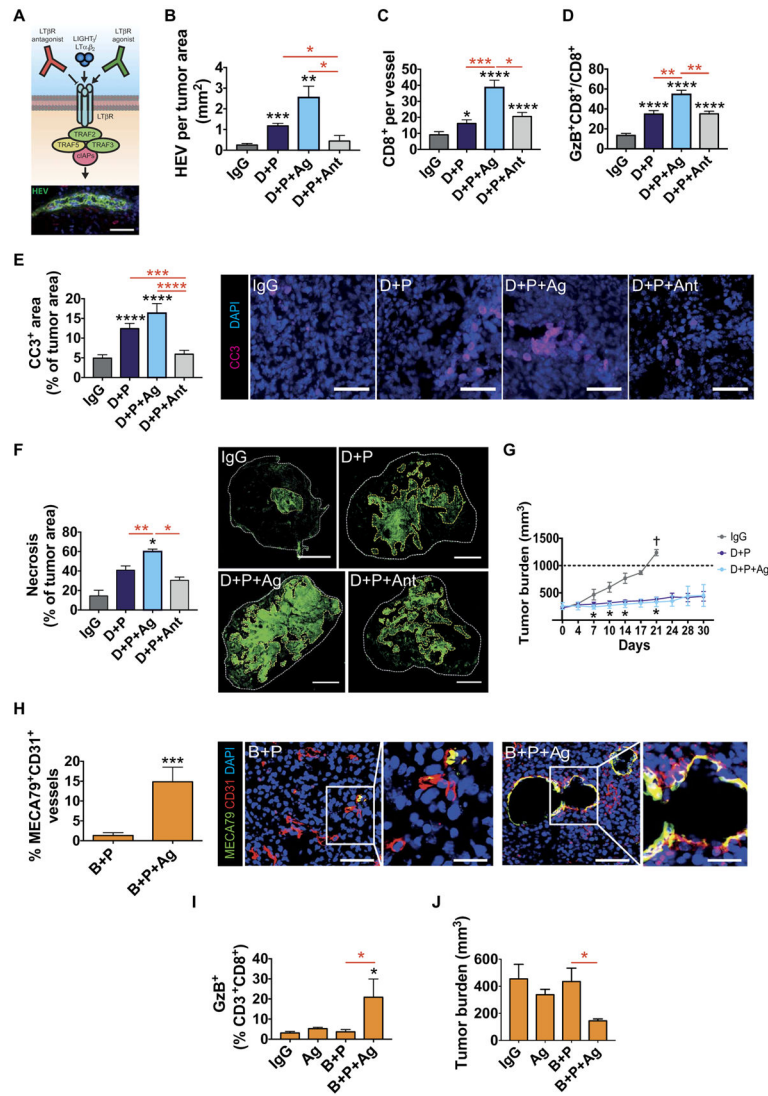


**Fig. 7. LT $\beta$ R-activation is implicated in HEV formation during antiangiogenic immunotherapy** (A) Top: Schematic of LT $\beta$ R effects with agonistic and antagonistic anti-LT $\beta$ R antibodies. Bottom: Image of an HEV. Scale bar, 50  $\mu$ m. (B to G) MMTV-PyMT mice were treated as indicated. (B) Number of HEVs per square millimeter of tumor area. IgG,  $n = 8$ ; D + P,  $n = 8$ ; D + P + agonistic anti-LT $\beta$ R (Ag),  $n = 5$ ; D + P + antagonistic anti-LT $\beta$ R (Ant),  $n = 5$ . (C) Number of CD8 $^{+}$  cells around tumor vessels. IgG,  $n = 21$ ; D + P,  $n = 18$ ; D + P + Ag,  $n = 39$ ; D + P + Ant,  $n = 18$ . (D) Number of GzB $^{+}$ CD8 $^{+}$  cells per field. IgG,  $n = 10$ ; D + P,  $n = 11$ ; D + P + Ag,  $n = 13$ ; D + P + Ant,  $n = 11$ . (E) Quantitation and visualization of CC3 $^{+}$  apoptotic cells. IgG,  $n = 25$ ; D + P,  $n = 20$ ; D + P + Ag,  $n = 27$ ; D + P + Ant,  $n = 26$ . Scale bars, 50  $\mu$ m. (F) Quantitation and visualization of necrotic areas in MMTV-PyMT tumors. IgG,  $n = 4$ ; D + P,  $n = 5$ ; D + P + Ag,  $n = 5$ ; D + P + Ant,  $n = 4$ . Scale bars, 1 mm. (G) Tumor size in PyMT mice under different treatment conditions. IgG,  $n = 4$ ; D + P,  $n = 4$ ; D + P + Ag,  $n = 4$ . (H) Quantitation and visualization of MECA79 $^{+}$ CD31 $^{+}$  tumor vessels in NFpp10-GBM tumors treated as indicated. B + P,  $n = 10$ ; B + P + Ag,  $n = 9$ . Scale bars, 50  $\mu$ m (low-magnification images); 20  $\mu$ m (high-magnification images). (I) FACS analysis of

GzB<sup>+</sup>CD3<sup>+</sup>CD8<sup>+</sup> CTLs under the different treatment conditions. IgG,  $n = 3$ ; Ag,  $n = 3$ ; B + P,  $n = 4$ ; B + P + Ag,  $n = 4$ . (J) Tumor burden of NFpp10-GBM mice under different treatment conditions. IgG and Ag,  $n = 3$ ; B + P and B + P + Ag,  $n = 4$ . Data are presented as means  $\pm$  SEM. \* $P < 0.05$ , \*\* $P < 0.01$ , \*\*\* $P < 0.001$ , and \*\*\*\* $P < 0.0001$  (for exact  $P$  values, see table S2); Mann-Whitney test. Black asterisks represent  $P$  values for comparisons between IgG and different treatments; red asterisks represent  $P$  values for other comparisons.